Nanoscale Advances

ROYAL SOCIETY OF CHEMISTRY

PAPER

View Article Online
View Journal | View Issue

Cite this: *Nanoscale Adv.*, 2020, **2**, 2363

Gold nanoclusters cause selective light-driven biochemical catalysis in living nano-biohybrid organisms†

John R. Bertram, ‡[ab] Yuchen Ding‡[bc] and Prashant Nagpal *[abc]

Living nano-biohybrid organisms or nanorgs combine the specificity and well-designed surface chemistry of an enzyme catalyst site, with the strong light absorption and efficient charge injection (for biocatalytic reaction) from inorganic materials. Previous efforts in harvesting sunlight for renewable and sustainable photochemical conversion of inexpensive feedstocks to biochemicals using nanorgs focused on the design of semiconductor nanoparticles or quantum dots (QDs). However, metal nanoparticles and nanoclusters (NCs), such as gold (Au), offer strong light absorption properties and biocompatibility for potential application in living nanorgs. Here we show that optimized, sub-1 nanometer Au NCs-nanorgs can carry out selective biochemical catalysis with high turnover number (10^8 mol mol^{-1} of cells) and turnover frequency (>2 $\times$ 10^7 h^{-1}). While the differences of size, light absorption, and electrochemical properties between these NCs (with 18, 22, and 25 atoms) are small, large differences in their light-activated properties dictate that 22 atom Au NCs are best suited for forming living nanorgs to drive photocatalytic ammonia production from air. Based on our experiments, these Au_{22} NC-nanorgs demonstrate 29.3% quantum efficiency of converting absorbed photons to the desired chemical, and 12.9% efficiency of photon-to-fuel conversion based on energy input–output. Further, by comparing the light-driven ammonia production yield between strains producing Mo–Fe nitrogenase with and without histidine tags, we demonstrate that preferential coupling of Au NCs to the nitrogenase through Au–histidine interactions is crucial for effective electron transfer and subsequent product generation. Together, these results provide the design rules for forming Au NCs-nanorgs and can have important implications for carrying out light-driven biochemical catalysis for renewable solar fuel generation.

Received 8th January 2020
Accepted 24th April 2020

DOI: 10.1039/d0na00017e

rsc.li/nanoscale-advances

Introduction

Biochemical conversion of inexpensive feedstocks like air, water, and carbon dioxide (CO_2) into desired chemicals and fuels offers specificity and low cost, but typically requires energetic substrates such as sugar to supply the energy required for conversion. Inorganic catalysts can directly utilize sunlight for photocatalytic conversion at high efficiencies, but suffers from lack of specificity.[1–3] Recently, nano-biohybrid catalysts have been suggested as an alternative, to combine the best properties of high turnover, efficiency, and selectivity, in a single biocatalyst both using *in vitro*[4–7] and *in vivo*[8–10] studies. Moreover, living or whole-cell biohybrids offer additional advantage of self-replication or growth, avoiding enzyme deactivation, and enzyme regeneration and repair. Living nano-biohybrid organisms, or nanorgs, combine these functionalities as a platform where targeted interfacial chemistry and specific enzyme attachment can be used to ensure facile uptake, self-assembly, and light-driven catalysis to specific chemicals or solar fuels.[10] Further, these nanorgs can use light-activated electrons from Au NCs to realize the production of ammonia from sunlight. These nanorgs do not rely on sugar as energy source, and can directly trigger an energetically uphill biocatalytic transformation of inexpensive substrates (air, CO_2) using wireless transfer of energy from light (or sunlight), for a range of selective biochemical or fuel generation as living microbial factories. To further advance nanorgs beyond semiconductor nanoparticles, here we demonstrate nanorgs made from small, sub-1 nanometer Au NCs.[11–15] Besides the biocompatibility of Au (to alleviate any environmental concerns due to use of heavy metals or material toxicity) and their large extinction coefficient,[16–18] the higher uptake (>92% uptake) and hence more efficient utilization of the added nanomaterials, the possibility of forming more enzyme biohybrids for better light-

[a]*Materials Science and Engineering, University of Colorado Boulder, USA. E-mail: pnagpal@colorado.edu*

[b]*Renewable and Sustainable Energy Institute (RASEI), University of Colorado Boulder, USA*

[c]*Department of Chemical and Biological Engineering, University of Colorado Boulder, USA*

† Electronic supplementary information (ESI) available: Formation of living bacteria nano-biohybrid (nanorgs) for light-induced fuel production, and additional figures. See DOI: 10.1039/d0na00017e

‡ J. R. B. and Y. D. contributed equally to the manuscript.

harvesting and enhanced solar-to-fuel conversion efficiency, this work will also serve to advance expanding the nanorg platform to a wide range of materials and microbial platforms.

Results and discussion

Design of atomically-precise Au NCs for forming nanorgs

In this work, we started our nanorgs design by screening different Au NCs because of their reported biocompatibility and potential impact in light-harvesting technologies.[19–22] We focused on Au NCs capped with the zwitterionic ligand, glutathione (GSH), due to their demonstrated low hydrodynamic radius for cellular uptake.[23–25] These atomically-precise Au NCs can be synthesized using simple wet-chemistry, with tunable optoelectronic properties (Fig. 1a), hydrodynamic size (Fig. 1b), surface charge (Fig. 1c), and electrochemical properties (Fig. 1d, and S1†) by modifying experimental factors like reaction pH, reducing agents, or reaction time (detailed in the ESI†). While all these glutathione-capped Au NCs have similar sub-1 nm size, their optoelectronic and electrochemical properties like HOMO–LUMO state energies, bandgaps *etc.* were slightly different. To further understand how these differences in light absorption, charge injection could affect the production yield, we focused on visible or near-infrared light-activated Au NCs with 18, 22, and 25 Au atoms (labeled as Au_{18}, Au_{22}, and Au_{25}). The nitrogen-fixing bacteria, *Azotobacter vinelandii*, were selected to couple to these Au NCs to form Au NC-*A. vinelandii* nano-biohybrids. Under visible light irradiation, photoexcited electrons (from Au NCs) with suitable redox potential can be directly injected into the nitrogenase in *A. vinelandii*, followed by conversion of dinitrogen to ammonia in ambient air (Fig. 1e).

Cellular uptake and biocompatibility of different-sized Au NCs

To allow direct electron transfer from light-activated Au NCs to the intracellular nitrogenase enzyme, cellular uptake and biocompatibility of these nanoclusters are required. Due to their extremely small sizes and favorable surface charge (zwitterionic), intracellular incorporation of these nanoclusters was as high as 90% (Fig. 2a). An additional merit of using the *A. vinelandii* DJ995 strain (produces a nitrogenase with a 7× histidine tag on the C-terminal of its α-subunit) is the strong Au NCs-nitrogenase coupling facilitated by the Au–histidine interactions (to be discussed later). Due to their similar hydrodynamic size and surface charge, these nanoclusters demonstrated similar cellular uptake for *A. vinelandii* (Fig. 2a). However, significant differences in their biocompatibility were observed, under dark and light-activated conditions. By treating *A. vinelandii* with Au_{22} NCs in dark or with light irradiation, we observed almost no effect on growth inhibition (as shown in the growth curves, Fig. 2b, and c), or loss of cell viability (after 5 hours light irradiation, as shown in the resazurin assay in Fig. 2d) even at very high NC concentration (up to 20 μM). Similarly, Au_{25} (Fig. 2b–d) and the smaller $Au_{10–12}$, Au_{15} NCs (Fig. S2†) demonstrate high biocompatibility with minor loss in cell viability. While *A. vinelandii* show no biocompatibility issues with Au_{18} NCs when treated in dark, light-treatment renders up to 80% growth inhibition and 95% loss of cell viability. This important difference indicates that Au_{18} NCs were not suitable for building living nanorgs. We hypothesize that the size-dependent and light/dark-dependent biocompatibility occurs as a direct result of the electrochemical potentials (specifically valence band position) and the light-generated holes by these Au NCs. Following photoexcitation, the photogenerated holes intracellularly using Au_{18} and Au_{15} NCs have extremely low VB positions (>+2 V *vs.* NHE, Fig. S1†) and therefore capable of quenching all electron injection and redox processes, and hence the metabolism in these cells. Spin-trapping EPR shows no reactive oxygen species (ROS) generation with these NCs under 400 nm light irradiation, which could explain their biocompatibility and lack of electron-induced toxicity. The phototoxicity of Au_{18} could be explained by their lower valence band, with unfavorable redox potential coupled to some vital cellular metabolism pathway. While smaller NCs ($Au_{10–12}$ and Au_{15}) with even lower valence band (hence stronger oxidation potency) should be more phototoxic. However, limited visible light absorption at this concentration was not able to generate enough photogenerated holes and therefore lower phototoxic effects. As we can see from Fig. S2,† some toxicity was observed with higher concentration smaller NCs, which proved that their biocompatibility is merely the result of limited light capture. Their lower yield in fuel production (described below, caused due to photogenerated electron injection) also supported this conclusion. Therefore, we focused on the more visible light-active Au_{18}, Au_{22}, and Au_{25} nanoclusters. By contrast, larger Au NCs (Au_{22} and Au_{25} NCs) had lower valence band and hence oxidation potentials, leading to negligible light-induced phototoxicity.

Role of biocompatibility and chemical coupling between Au NCs-enzymes in nanorgs

To further probe the effect of cell viability and coupling chemistry between Au NCs and nanorg enzymes, we carried out light-driven ammonia production using these Au NCs-*A. vinelandii* nanorgs in sugar-free media. This reaction relies on the injection of light-induced electrons from Au NCs to the nitrogenase in the bacteria cells. Since nitrogenase is extremely sensitive to oxygen and is normally protected inside living cells, loss of cell viability could render the complete or partial loss of enzyme activity if rendered in air.[4,10,26,27] In order to verify this and correlate the cell viability with product yield, we compared the photocatalytic ammonia turnover number carried out in air (contains dinitrogen and dioxygen) and pure dinitrogen (oxygen-free). Using respective ammonia yield performed in pure dinitrogen as a reference, no change of ammonia production was observed in air with nanorgs made from Au_{22} NCs, while the ammonia turnover number with Au_{18} NCs decreased to 30% of the yield in dinitrogen (Fig. 3a). The decrease of ammonia yield in air using nanorgs built from Au_{18} NCs corresponds to the loss of cell viability, whose nitrogenase is partially deactivated by oxygen in air. Similar control experiments were performed in an argon atmosphere, and no detection of ammonia indicates the dinitrogen as the sole nitrogen

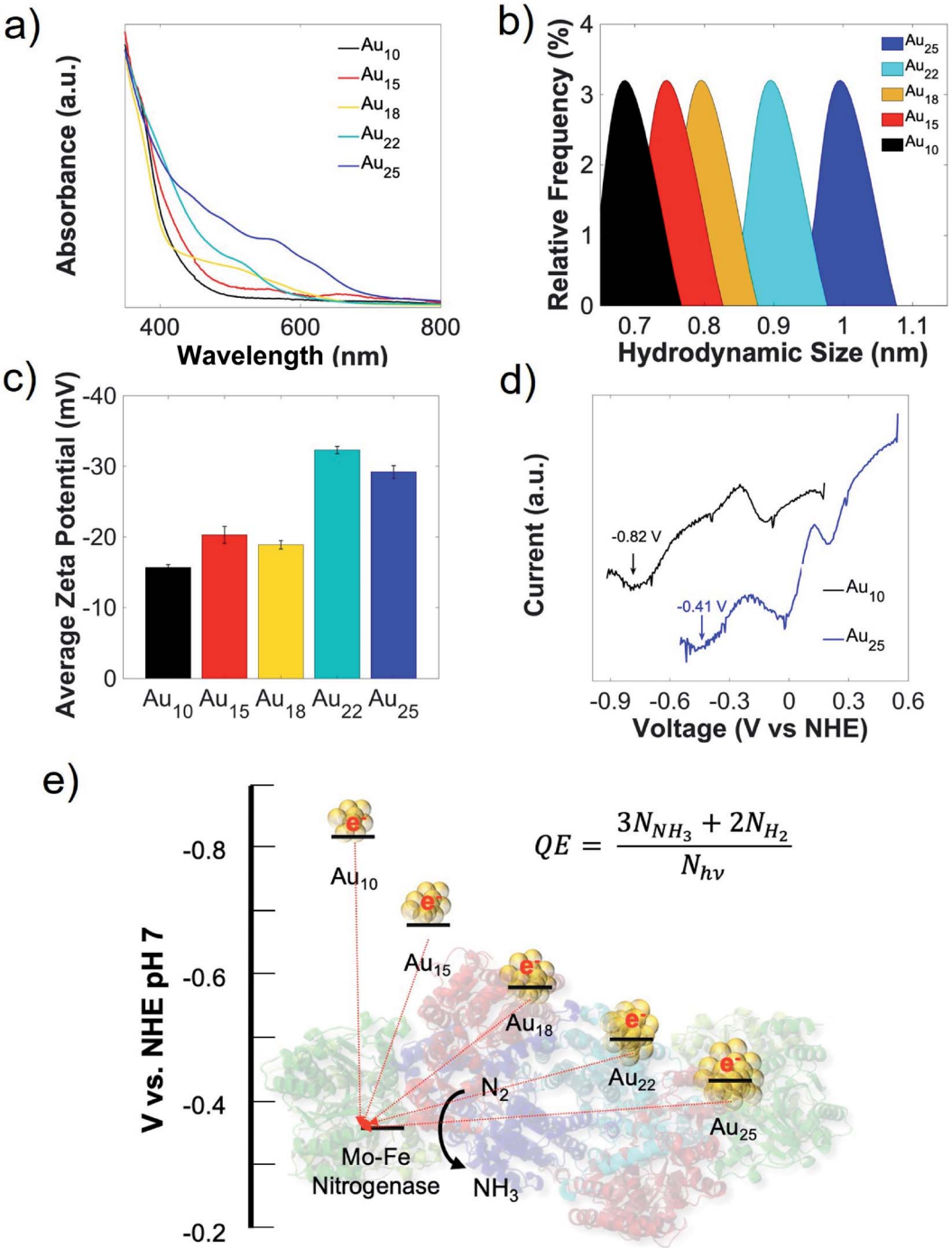

Fig. 1 Selection of different atomically-precise Au NCs for forming nanorgs. (a) Ultraviolet-visible (UV-Vis) spectra, (b) hydrodynamic size (measured by dynamic light scattering), (c) zeta potential, (d) redox potential (showing the conduction band, measured by differential pulse voltammetry) of different-sized Au NCs. (e) Schematic diagram of electron transfer from light-activated Au NCs to nitrogenase for dinitrogen reduction to ammonia, with energy levels for different Au NCs conduction band and Mo–Fe nitrogenase reduction potential.

source instead of the reaction media or the bacteria cellular components for ammonia production. Other control tests, including the removal of light, removal of cells, and Au NCs, were conducted to prove the generation of ammonia from light-driven enzymatic conversion in these nanorgs (Table S1†). To probe the effect of coupling chemistry between Au NCs and enzymes on nanorg biocatalytic conversion, we compared the light-driven ammonia production performance using the optimal Au_{22} NCs with different *A. vinelandii* strains (Fig. 3b). As mentioned previously, we selected the DJ995 strain that produces a nitrogenase with a 7× histidine tag to facilitate its coupling to the Au NCs (using Au–histidine interactions). This

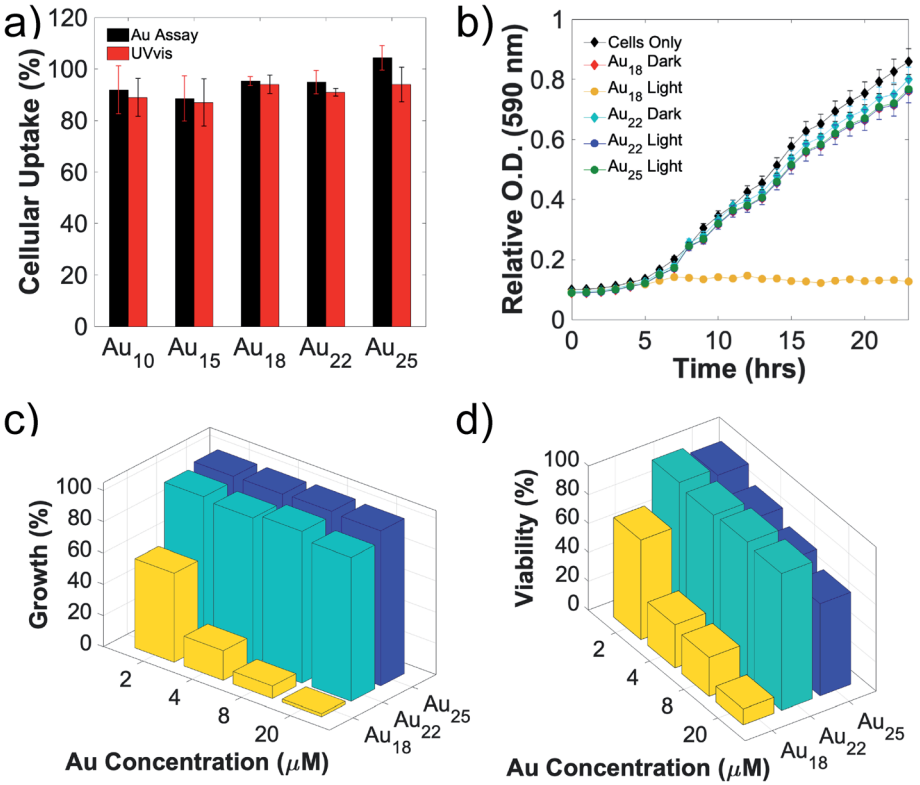

Fig. 2 Cellular uptake and biocompatibility of Au NCs. (a) Cellular uptake of different sized Au NCs by *A. vinelandii*, performed using Au elemental analysis (black histograms) and UV-Vis spectroscopy of the Au NCs (red histograms). (b) *A. vinelandii* growth curve with different sized 20 μM Au NCs, incubated in dark and with light irradiation. (c) A 3D plot showing the percentage of growth (compared to cell growth with no Au NCs as 100%) under light irradiation, calculated from the corresponding growth curves at 24 hours time point. (d) Resazurin dye assay to evaluate the cell viability after 4 hours Au NCs treatment under light irradiation. Viability is calculated using treatment with no Au NCs as reference (100%).

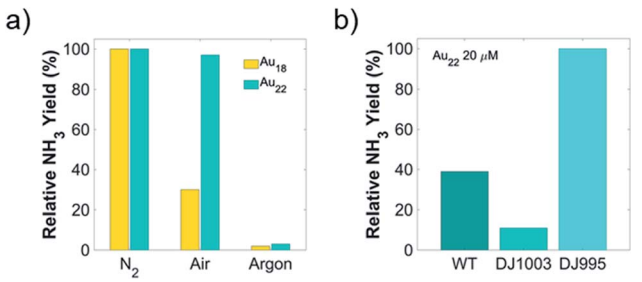

Fig. 3 Influence of biocompatibility and chemical coupling between Au NCs-enzymes in nanorgs. Light-driven ammonia production (a) using nanorgs constructed from Au_{18} or Au_{22} NCs with *A. vinelandii* DJ995 strain, conducted in different atmospheres; and (b) using nanorgs constructed from Au_{22} NCs with different *A. vinelandii* strains.

His-tag is located on the C-terminus of the α-subunit of the MoFe nitrogenase enzyme. In natural conditions, Fe protein that attached to the MoFe nitrogenase act as a mediator to transfer energetic electrons to the P-cluster and finally to the FeMo-cofactor reaction center for dinitrogen reduction to ammonia. Due to the close distance between His-tag and P-cluster/FeMo-cofactor, direct electron injection from light-activated Au NCs are expected. As a comparison, a wild-type strain (*A. vinelandii* Wards) with no such affinity was also used to form the nanorgs. Under the same photocatalytic tests, their ammonia yield is only half compared to our optimized systems, which could be explained by the poor electron transfer from the Au_{22} to the nitrogenase due to unfavorable coupling between them. This again highlights the importance of (specific) coupling between the Au NCs and the enzyme for effective fuel production, as reported previously in the CdS/ZnS QDs-His-tagged nitrogenase biohybrids.[10] Similar tests were also conducted on nanorgs made from *A. vinelandii* DJ1003 strain, which produces an apo-nitrogenase (also with histidine-tag) that lacks the essential Mo–Fe cofactors for nitrogen fixation. As expected, a negligible amount of ammonia was produced.

Light-driven biocatalytic reaction efficiency using nanorgs from different Au NCs

To optimize the turnover number, turnover frequency, and the photon-to-chemical conversion yield (quantum yield, QY), we conducted concentration-dependent light-driven air–water reduction reaction with different Au NCs-*A. vinelandii* nanorgs. Kinetics of ammonia production indicates no loss of nanorg viability or nitrogenase activity for more than 4 hours in Au_{22} NC nanorgs (Fig. 4a), as shown in an almost linear increase of ammonia turnover number with time. The initial increase of ammonia turnover number with increasing Au_{22} NCs concentration (Fig. 4b) can be explained by more efficient light capture

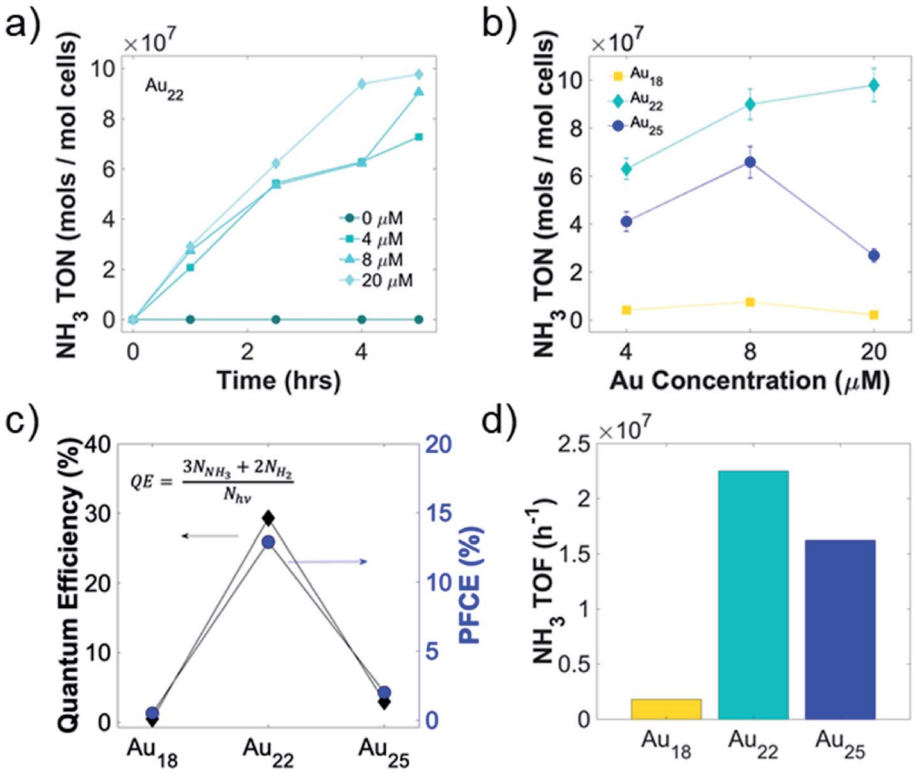

Fig. 4 Light-driven biocatalytic reaction efficiency using nanorgs from different Au NCs. (a) Time-dependent ammonia production with Au_{22} NC-nanorgs. (b) A 3D plot showing the ammonia turnover number using nanorgs made from different Au NCs at different concentrations. (c) Calculated quantum efficiency (QE) and photon-to-fuel conversion efficiency (PFCE) of each optimized nanorgs. (d) Ammonia turnover frequency using nanorgs made from different Au NCs (8 μM).

and electron generation. However, as more Au_{22} NCs are added, an insignificant increase of ammonia turnover number beyond 8 μM Au_{22} NCs could be attributed to the intracellular nitrogenase bottleneck, where all available enzymes are coupled to the NCs. Similarly, nanorgs made from Au_{25} NCs show an initial increase of ammonia yield with NC concentration due to improved electron supply from light-activated NCs, while a significant decrease of yield with 20 μM NCs is most likely caused by viability loss issues, which is also the reason of overall low ammonia yield for nanorgs made from Au_{18} NCs. As for nanorgs made from Au_{10-12} and Au_{15} NCs, low ammonia yield (Fig. S3†) could be explained by insufficient visible light absorption. Using the optimized conditions in nanorgs made from Au_{18}, Au_{22}, and Au_{25} NCs, the highest ammonia turnover frequency (Fig. 4d) of $>2 \times 10^7$ h^{-1} can be realized. To further quantify the conversion efficiencies, the photon-to-fuel conversion efficiency (PFCE) and quantum efficiency (QE) were calculated (Fig. 4c), by considering the total photon absorbed by the nanorgs and the final electrons resulting in ammonia and hydrogen generation (Fig. S4†). To calculate the QE of this process, we first estimated the number of photons absorbed by the nanorgs (assuming complete saturation of all nitrogenase enzymes, $\sim 3.83 \times 10^{13}$ photons per s, detailed calculations in ESI†). Comparing this to the number of electrons used for fuel generation (3 for each NH_3 molecules, 2 for each H_2 molecule, with NH_3 and H_2 turnover frequency of 6250 and 3075 s^{-1}, respectively), we estimated the total electron flux for biocatalytic fuel generation to be $\sim 1.12 \times 10^{13}$ s^{-1}, resulting in a QE 29.3%. To further estimate the photons-to-fuel conversion efficiency generation using enzyme activation with light, limited by enzyme turnover rate,[10] the energy input from light was estimated to be 18.9 μJ and energy output obtained from fuels was 2.445 μJ mL^{-1} of O.D. 1 nanorg suspension. This leads to PFCE of 12.9% (Fig. 4c, detailed calculations in ESI†). Therefore, this light-driven enzyme activity (zero in dark, and close to thermodynamic efficiency/enzyme turnover frequency on light irradiation) also provides a valuable tool to precisely control the enzyme activity of each enzyme individually using focused light (using either optics, or combined with multiphoton absorption in Au NCs/QDs), or controlling light intensity, thereby providing unprecedented control over single-enzyme sites for fine-tuning the enzyme activity, without changing the genetics/synthetic biology, or chemical changes to the cell. The QE of 29.3% and PFCE of 12.9% (Fig. 4c) indicates a highly efficient photon-to-fuel conversion system (comparable to solar cells) by combining efficacies of both high-efficiency light-sensitizer and high-selectivity enzymatic systems.

Mechanism of selective light-driven biochemical catalysis in living Au NC nano-biohybrid organisms

To summarize our design and mechanistic insights obtained from our experiments, the selective light-driven biochemical

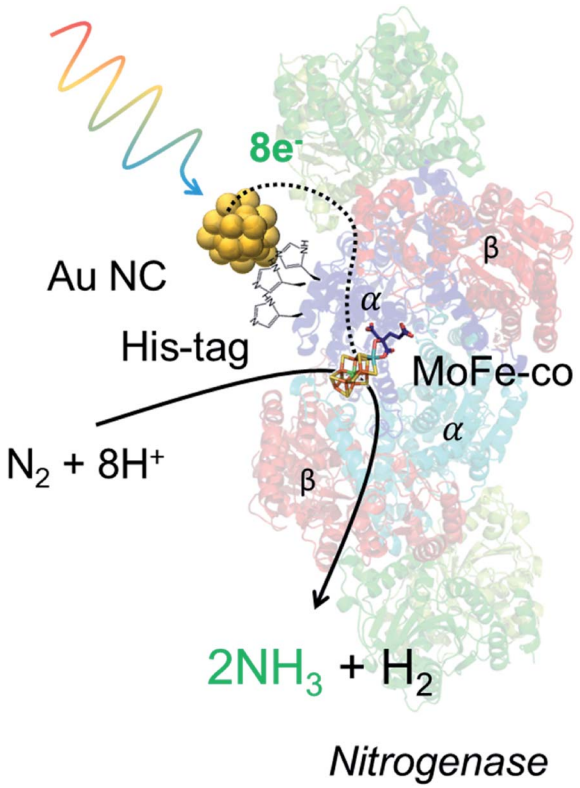

Fig. 5 Mechanism of selective light-driven biochemical catalysis in living Au NC nano-biohybrid organisms. The schematic showing the mechanism of selective light-driven biochemical catalysis using Au NCs. The Au NCs attached to the histidine-tagged enzyme (alpha Mo–Fe nitrogenase cofactor in *Azotobacter vinelandii* here) absorb light and inject electrochemically matched photogenerated electrons to the reaction site. These electrons cause dinitrogen–water reduction, to give ammonia and hydrogen.

catalysis is carried out by Au NCs in nano-biohybrid organisms (Fig. 5). The Au NCs attach selectively to the histidine-tagged enzyme (Fig. S7†), α Mo–Fe nitrogenase sub-unit in *A. vinelandii* here, to absorb light and inject the photogenerated electron to the electrochemically matched reaction site. These electrons cause dinitrogen–water reduction, to give ammonia and hydrogen at high turnover number, high turnover frequency, high selectivity, low overpotential, and resulting high efficiency for light-to-fuel conversion on an energy basis (~13%). Since this solar-to-chemical conversion efficiency can be as efficient as novel solar cells, these nano-biohybrid organisms can function at low cost and generate fuel and chemicals for later use, obviating the need for a separate energy storage mechanism or changes to existing energy infrastructure, providing a low-cost, highly efficient, and practical alternative to renewable and sustainable energy production.

Conclusion

In conclusion, we have demonstrated light-driven biochemical catalysis using Au NC-*A. vinelandii* living nano-biohybrids (nanorgs), with a high turnover number (10^8 mol mol^{-1} of cells) and turnover frequency (>2×10^7 h^{-1}) for ammonia production in ambient air. By screening different atomically-precise Au NCs capped with zwitterionic ligand glutathione, we have selected the best candidate, Au_{22} NCs, combining desired properties of high cellular uptake, effective light capture, suitable redox potential for electron transfer, and non-toxicity/biocompatibility, for building the nanorgs. In addition, the coupling of Au NCs to the His-tagged nitrogenase produced by *A. vinelandii* DJ995 strain demonstrates the importance of strong histidine–Au binding for high-efficiency biocatalytic applications. The optimized system can yield a high turnover frequency >2×10^7 h^{-1}, with photon-to-fuel conversion efficiency (PFCE yield of 12.9%). Since such high turnover number and frequency is difficult to achieve using conventional synthetic tools and such precise control over individual enzyme activity is not possible with most energetic substrates/conventional substrate-driven enzymatic catalysis, it could provide a new pathway for potentially better design of or high-throughput optimization of such biocatalytic reaction in optimized microbial systems. Together, these results can pave the way for expanding the choice of available benign and biocompatible materials with high absorption cross-sections, and optimized microbes for building living nanorgs that can have important implications for carrying out light-driven biochemical catalysis for renewable solar fuel generation.

Experimental method

Synthesis of glutathione-capped gold nanoclusters (NCs)

Atomically-precise gold NCs capped with glutathione (GSH) capping ligands were synthesized based on the methods reported by Zhang *et al.*, and Kamat *et al.*[13–16,18–22,28]

Au_{18} NCs were synthesized by dissolving 150 mg $HAuCl_4 \cdot 3H_2O$ in 1.2 mL methanol and adding 1.8 mL DI water. 300 mg of glutathione was added to this solution and sonicated to dissolve. Once the glutathione dissolved and the color changed from yellow to almost colorless. 96 mL methanol was then added and stirred for 10 min. 4.5 mL of a 220 mM $NaBH_3CN$ solution was added under vigorous stirring for 30 min. After 30 min the precipitate was removed by centrifugation and washed with methanol repeatedly to remove any remaining precursor. Finally, the precipitate was dissolved in water and freeze-dried to obtain a pale red powder identified as $Au_{18}SG_{14}$.

Au_{22} NCs were prepared by mixing 12.5 mL 20 mM $HAuCl_4$ and 7.5 mL 50 mM glutathione solution in a 500 mL flask containing 180 mL of DI water. After vigorously stirring for 2 min, the pH was raised to 12.0 with 1 M NaOH, after which 0.24 mg $NaBH_4$ in 0.1 mL DI water was added to the reaction with sitting at 500 rpm. After 30 min, the pH was lowered to 2.5 with 0.33 M HCl. The reaction solution was then sealed airtight with stirring at 200 rpm and allowed to react for 8 hours forming a red-emitting Au_{22} solution. The NCs were cleaned by using isopropyl alcohol and centrifugation and finally resuspended in water and kept in the fridge away from light for future use.

$Au_{10–12}$, Au_{15}, and Au_{25} NCs were synthesized by carbon monoxide (CO) reducing techniques. Briefly, in a 125 mL flask with 20 mL distilled water, 100 mM $HAuCl_4$ and 200 mM reduced

glutathione were added to a final concentration of 1 mM and 2 mM, respectively. The pH of the mixture was adjusted to 7, 9, and 11 for Au_{10-12}, Au_{15}, and Au_{25} NCs synthesis, respectively. The flask was sealed with a rubber septum and flush with pure CO gas through a syringe needle for 2 min. The mixture was violently stirred for 24 hours and the resulting Au NCs were precipitated with an excess amount of isopropanol, followed by separating with centrifugation at 5000 rpm. The precipitates were dried with clean air and re-suspend in distilled water. The Au NCs were stored at 4 °C for future tests.

Characterization of Au NCs

Ultraviolet-visible (UV-Vis) spectra were measured using the UV1600PC UV-Vis spectrometer (VWR). Litesizer 500 (Anton-Paar) was used to perform dynamic light scattering (DLS) and zeta-potential measurements to estimate the hydrodynamic size and zeta potential of the Au NCs. Samples were prepared by taking a 0.5 mL aliquot of the freshly washed NCs and diluting with DI water until the solution just became translucent. The pH of each sample was then adjusted to physiological pH (~7.4)

The conduction band (CB) of the NCs was characterized using differential pulse voltammetry (DPV), with a Bio-logic SP200 potentiostat. A three-electrode configuration with a 3 mm glassy carbon working electrode, a platinum wire counter electrode, and a Ag/AgCl reference electrode was used. Au NCs suspension (in 0.1 M Na_2SO_4 electrolyte) was bubbled with argon for 10 min before the measurement. DPV was taken with the following parameters: 50 ms pulse width, 50 mV pulse height, 200 ms step width, and 4 mV step height (~20 mV s^{-1} scan rate).

Native polyacrylamide gel electrophoresis (PAGE) of Au NCs

Native PAGE was used to characterize the purity of these Au NCs, which was carried out using the Mini-PROTEAN Tetra Handcast system (Biorad Inc.). Stacking and Resolving gels were prepared from 5% and 30% acrylamide monomers (monomer : cross-linker = 19 : 1). The electrophoresis buffer was made of 192 mM glycine and 25 mM tris(hydroxymethyl)aminomethane (Tris). 60 μL Au NCs were mixed with 20 μL 50% glycerol solution and 10 μL of the above mixture was loaded onto the wells. Electrophoresis was performed at a constant 250 V voltage at room temperature for several hours. From the resulting gel (Fig. S8†), we can clearly see a single band for Au_{15}, Au_{18}, and Au_{25} nanoclusters, indicating their high purity from the synthesis mentioned above. For Au_{22} NCs, we have also observed one band from Au_{25} NCs, indicating some Au_{25} NCs impurities in these Au_{22} NCs. However, this will not affect our results due to their similar light-capturing capability, cellular uptake, and biocompatibility (detailed in the main text). We have observed different bands from the gel, indicating the formation of NCs with different sizes and compositions. Gold nanoclusters synthesized in this manuscript are relatively pure, which can be directly used without the need for further separation.

Preparation of *A. vinelandii* culture

A. vinelandii DJ995 and DJ1003 strain were kindly provided by the Dennis group (Virginia Tech). Modifications to obtain these strain variations were accomplished *via* site-directed mutagenesis and gene-replacement techniques.[27] Typically, bacteria were grown in nitrogen-limited Burk media (with 3 mM urea) at 30 °C, with 200 rpm shaking. Cultures at an optical density (OD) ~1.5 (overnight culture) were collected for future tests.

Cell growth curve and viability tests

Cell growth curves and resazurin assays were performed in Burk media and photocatalytic media, respectively, with a variation of Au NC size. *A. vinelandii* DJ995 was first grown in nitrogen-free Burk media and harvested near OD 1.5, washed twice and resuspended in photocatalytic media. The cells and their respective NCs were then incubated and subject to light-exposure to produce NH_3. After production was complete (~4 h) the nanorg mixtures were subject to both growth and viability measurements. The cell growth curves were taken in a 96-well microplate at 30C with vigorous shaking and monitored using a microplate reader (TECAN GENios) controlled by Megellan 7.2 software. An initial OD of 0.1 in Burk media was used for the growth curves. The resazurin assay was performed separately in a 96-well plate with the bacteria maintained at an OD of 1.0 after the photocatalytic tests. Resazurin was added to a final concentration of 0.1 mg mL^{-1} and the fluorescence was measured at 620 nm (485 excitation) over the course of 2 hours.

Cellular uptake

Uptake of Au NCs by *A. vinelandii* was determined by a UV-Vis spectrophotometric method. NCs first had their UV-Vis spectra recorded in photocatalytic media at the desired concentration (20 μM). The initial absorption value at the first excitonic peak was taken to be the 0% uptake mark (Abs_i). Then the NCs at the desired concentration (20 μM) were incubated with the bacteria at OD 1.0 in photocatalytic media for 15 minutes on a shaker at 250 rpm. The mixtures were then centrifuged at 5000 rpm and aliquots of the supernatant were taken for UV-Vis measurement. The absorption values of the supernatant at the corresponding excitonic peak position (Abs_f) were used to calculate the uptake% using the following equation:

$$\text{Uptake}\% = \frac{\text{Abs}_i - \text{Abs}_f}{\text{Abs}_i} \times 100\%$$

Uptake was also quantified by elemental analysis of gold ion (Au(III)) using a colorimetric assay.[29] Briefly, *aqua regia* (~20 μL) was added to 200 μL of the above supernatant. After incubating for 30 min, the pH of the solution was adjusted to ~3.5 using NaOH, followed by dilution to 1 mL. 0.2 mL of the assay solution (2 mM 3,3′,5,5′-tetramethylbenzidine (TMB) in a mixture of ethanol and NaAc/HAc buffer (1 M, pH = 3.5) at a volume ratio of 4 : 1). After 3 min incubation, UV-Vis spectra of the mixture were taken (Abs_f). The same assay was also performed on Au NCs incubating in the photocatalytic media without the addition of cells (Abs_i). The same calculation is used to quantify the cellular uptake of Au NCs.

Light-driven ammonia production and ammonia assay

Ammonia production with the nanorgs was achieved by first growing *A. vinelandii* to an OD of ~1.5 in Burk media. The cells were then washed twice with sugar-free photocatalytic media (25 mM ascorbic acid 35 mM HEPES) to remove any residual sugars. Cells were then resuspended in photocatalytic media and diluted to a final OD of 1.0. Data with NH_3 production in the absence of ascorbic acid is shown in Fig. S5.† The Au NCs were then added to the bacteria and allowed to incubate for 15 min before subjecting to production. For production, the nanorgs were subjected to light irradiation (400 nm LED, 1.6 mW cm^{-2}) for 5 hours on a shaker at 250 rpm. 25 μL aliquots were taken at various time points throughout the reaction to monitor the kinetics.

Ammonia was quantified using a fluorescent assay described previously.[10] Typically, 25 μL sample (cells were first lysed using ultrasonication) was added to 0.5 mL *o*-phthalaldehyde assay reagent and incubated in dark for 30 min, followed by measuring the fluorescence at 472 nm (excitation at 410 nm). Each sample was compared against a control that was shielded from light throughout the experiment to monitor the net amount of ammonia generated. A representative calibration curve (Fig. S6†), as well as representative data illustrating how the calculations were carried out (Table S1†), are presented in the ESI.†

Conflicts of interest

The authors declare no competing financial interests.

Acknowledgements

The work was funded by the Department of Energy (DOE), Biological and Environmental Research (BER), Award DE-SC0020361.

References

1 R. E. Blankenship, D. M. Tiede, J. Barber, G. W. Brudvig, G. Fleming, M. Ghirardi, M. R. Gunner, W. Junge, D. M. Kramer, A. Melis, T. A. Moore, C. C. Moser, D. G. Nocera, A. J. Nozik, D. R. Ort, W. W. Parson, R. C. Prince and R. T. Sayre, *Science*, 2011, **332**, 805–809.
2 A. M. Appel, J. E. Bercaw, A. B. Bocarsly, H. Dobbek, D. L. Dubois, M. Dupuis, J. G. Ferry, E. Fujita, R. Hille, P. J. A. Kenis, C. A. Kerfeld, R. H. Morris, C. H. F. Peden, A. R. Portis, S. W. Ragsdale, T. B. Rauchfuss, J. N. H. Reek, L. C. Seefeldt, R. K. Thauer and G. L. Waldrop, *Chem. Rev.*, 2013, **113**, 6621–6658.
3 K. K. Sakimoto, N. Kornienko and P. Yang, *Acc. Chem. Res.*, 2017, **50**, 476–481.
4 K. A. Brown, D. F. Harris, M. B. Wilker, A. Rasmussen, N. Khadka, H. Hamby, S. Keable, G. Dukovic, J. W. Peters, L. C. Seefeldt and P. W. King, *Science*, 2016, **352**, 448–450.
5 R. D. Milton, S. Abdellaoui, N. Khadka, D. R. Dean, D. Leech, L. C. Seefeldt and S. D. Minteer, *Energy Environ. Sci.*, 2016, **9**, 2550–2554.
6 R. D. Milton, R. Cai, S. Sahin, S. Abdellaoui, B. Alkotaini, D. Leech and S. D. Minteer, *J. Am. Chem. Soc.*, 2017, **139**, 9044–9052.
7 R. Cai, R. D. Milton, S. Abdellaoui, T. Park, J. Patel, B. Alkotaini and S. D. Minteer, *J. Am. Chem. Soc.*, 2018, **140**, 5041–5044.
8 K. K. Sakimoto, A. B. Wong and P. Yang, *Science*, 2016, **351**, 74–77.
9 H. Zhang, H. Liu, Z. Tian, D. Lu, Y. Yu, S. Cestellos-Blanco, K. K. Sakimoto and P. Yang, *Nat. Nanotechnol.*, 2018, **13**, 900–905.
10 Y. Ding, J. R. Bertram, C. Eckert, R. R. Bommareddy, R. Patel, A. Conradie, S. Bryan and P. Nagpal, *J. Am. Chem. Soc.*, 2019, **141**, 10272–10282.
11 Y. Negishi, Y. Takasugi, S. Sato, H. Yao, K. Kimura and T. Tsukuda, *J. Am. Chem. Soc.*, 2004, **126**, 6518–6519.
12 Y. Negishi, K. Nobusada and T. Tsukuda, *J. Am. Chem. Soc.*, 2005, **127**, 5261–5270.
13 J. Zheng, C. Zhang and R. M. Dickson, *Phys. Rev. Lett.*, 2004, **93**, 077402.
14 J. Zheng, P. R. Nicovich and R. M. Dickson, *Annu. Rev. Phys. Chem.*, 2007, **58**, 409–431.
15 L. Y. Chen, C. W. Wang, Z. Yuan and H. T. Chang, *Anal. Chem.*, 2015, **87**, 216–229.
16 E. C. Dreaden, A. M. Alkilany, X. Huang, C. J. Murphy and M. A. El-Sayed, *Chem. Soc. Rev.*, 2012, **41**, 2740–2779.
17 R. Shukla, V. Bansal, M. Chaudhary, A. Basu, A. Ramesh, R. Bhonde and M. Sastry, *Langmuir*, 2005, **21**, 10644–10654.
18 C. Zhou, M. Long, Y. Qin, X. Sun and J. Zheng, *Angew. Chem., Int. Ed.*, 2011, **50**, 3168–3172.
19 Y. Yu, Z. Luo, D. M. Chevrier, D. T. Leong, P. Zhang, D. E. Jiang and J. Xie, *J. Am. Chem. Soc.*, 2014, **136**, 1246–1249.
20 M. A. Abbas, P. V. Kamat and J. H. Bang, *ACS Energy Lett.*, 2018, **3**, 840–854.
21 X. D. Zhang, Z. Luo, J. Chen, S. Song, X. Yuan, X. Shen, H. Wang, Y. Sun, K. Gao, L. Zhang, S. Fan, D. T. Leong, M. Guo and J. Xie, *Sci. Rep.*, 2005, **5**, 8669.
22 A. Mathew and T. Pradeep, *Part. Part. Syst. Charact.*, 2014, **31**, 1017–1053.
23 H. S. Choi, W. Liu, P. Misra, E. Tanaka, J. P. Zimmer, B. I. Ipe, M. G. Bawendi and J. V Frangioni, *Nat. Biotechnol.*, 2007, **25**, 1165–1170.
24 S. M. Goodman, M. Levy, F. F. Li, Y. Ding, C. M. Courtney, P. P. Chowdhury, A. Erbse, A. Chatterjee and P. Nagpal, *Front. Chem.*, 2018, **6**, 46.
25 M. Levy, P. P. Chowdhury and P. Nagpal, *J. Biol. Eng.*, 2019, **13**(13), 48.
26 B. M. Hoffman, D. Lukoyanov, Z. Y. Yang, D. R. Dean and L. C. Seefeldt, *Chem. Rev.*, 2014, **114**, 4041–4062.
27 J. Christiansen, P. J. Goodwin, W. N. Lanzilotta, L. C. Seefeldt and D. R. Dean, *Biochemistry*, 1998, **37**, 12611–12623.
28 R. Shukla, V. Bansal, M. Chaudhary, A. Basu, R. R. Bhonde and M. Sastry, *Langmuir*, 2005, **21**, 10644–10654.
29 X. Xia, J. Zhang and T. Sawall, *Anal. Methods*, 2015, **7**, 3671–3675.